Journal of Scientific Computing (2023) 95:96
https://doi.org/10.1007/s10915-023-02222-5

Quadrature by Two Expansions for Evaluating Helmholtz Layer Potentials

Jared Weed[1] · Lingyun Ding[2] · Jingfang Huang[2] · Min Hyung Cho[1]

Received: 27 July 2022 / Revised: 18 April 2023 / Accepted: 25 April 2023

Abstract
In this paper, a Quadrature by Two Expansions (QB2X) numerical integration technique is developed for the single and double layer potentials of the Helmholtz equation in two dimensions. The QB2X method uses both local complex Taylor expansions and plane wave type expansions to achieve a resulting representation which is numerically accurate for all target points inside a leaf box in the fast multipole method (FMM) hierarchical tree structure. The QB2X method explicitly includes nonlinear dependency of the boundary geometry in the plane wave expansions, thereby providing for higher-order representations of both the boundary geometry and density functions in the integrand, with its convergence following standard FMM error analysis. Numerical results are presented to demonstrate the performance of the QB2X method for Helmholtz layer potentials using one expansion center for the entire FMM-leaf box for both flat and curved boundaries with various densities.

Keywords Layer potentials · Quadrature by two expansions · Quadrature by expansion · Helmholtz equation · Integral equations

Mathematics Subject Classification (2000) 65R20 · 65D30 · 65E05 · 65T40 · 31C05 · 32A55 · 41A10

✉ Min Hyung Cho
minhyung_cho@uml.edu

Jared Weed
Jared_Weed@student.uml.edu

Lingyun Ding
dingly@live.unc.edu

Jingfang Huang
huang@email.unc.edu

[1] Department of Mathematical Sciences, University of Massachusetts Lowell, Lowell, MA 01854, USA

[2] Department of Mathematics, University of North Carolina at Chapel Hill, Chapel Hill, NC 27599, USA

Published online: 15 May 2023

1 Introduction

Applying classical potential theory of partial differential equation (PDE) analysis, the solution for the homogeneous Helmholtz equation

$$\Delta u + k^2 u = 0 \tag{1}$$

with a given boundary condition on the boundary Γ can be represented as the linear combinations of single and double layer potentials

$$S\psi(w) = \int_\Gamma G(w,z)\psi(z)\mathrm{d}z \text{ and } D\psi(w) = \int_\Gamma \frac{\partial G(w,z)}{\partial \mathbf{n}_z}\psi(z)\mathrm{d}z, \tag{2}$$

where k is the wave number, $G(w,z) = \frac{\mathrm{i}}{4}H_0^{(1)}(k|w-z|)$ is the free-space Green's function at the target point w due to the source point z on the boundary, $H_0^{(1)}$ denotes the 0^{th} order Hankel function of the first kind, $\mathbf{n}_z$ is the outward normal vector at z, and ψ is the unknown density function (may be different for single and double layer potentials) on the boundary. To satisfy the given boundary condition, a common practice with integral equation methods is to find an appropriate combination of the layer potentials and derive a well-conditioned Fredholm second-kind boundary integral equation for the unknown density functions. Then, proper quadrature rules are applied to discretize the continuous integral equation formulation and yield a system of linear algebraic equations which can be solved by either fast direct or iterative solvers. One of the main numerical challenges with this process is the accurate and efficient evaluation of layer potentials with singular or nearly-singular kernels, especially when the target point w is close to, or on the boundary of Γ. Note that the target point is located exactly on the boundary in the boundary integral equation formulation, and in applications such as near-field optics [1], surface plasmon resonance [2], and meta-materials [3], the solution near the boundary plays an important role in determining the physical properties of the system. Numerical integration quadrature rules for singular and nearly-singular integrals have been extensively studied in literature. One technique is to modify the classical Newton-Cotes or Gaussian quadrature rules, either locally or globally, to compensate for the singularity in the kernel. The resulting schemes include an Alpert quadrature [4], a Rokhlin-Kapur quadrature [5], a zeta correction quadrature [6], and a generalized Gaussian quadrature [7, 8]. Other techniques involve analytically removing singularities using a change of variables [9, 10] or a regularization-correction method [11]. Some of these quadrature techniques only work when the target point is located exactly on the boundary, and the performance of most existing quadrature rules depends on the complexity of the boundary geometry and distance between the target point and boundary Γ, which determines the kernel's singularity features.

By utilizing the smoothness properties of the layer potentials respectively in the interior and exterior of the domain, along with special partial wave or local expansions which automatically satisfy the underlying partial differential equations, the pioneering "quadrature by expansion" (QBX) scheme is introduced [12]. The partial wave (harmonics) expansion valid in a region close to (or even containing points on) the boundary is derived as

$$\phi(w) = \sum_{n=-\infty}^{\infty} \alpha_n J_n(k||w-c||)e^{-\mathrm{i}n\theta}, \tag{3}$$

where

$$\alpha_n = \frac{\mathrm{i}}{4}\int_\Gamma H_n^{(1)}(k|z-c|)e^{\mathrm{i}n\theta_z}\psi(z)\mathrm{d}z \text{ for the single layer potentials,}$$

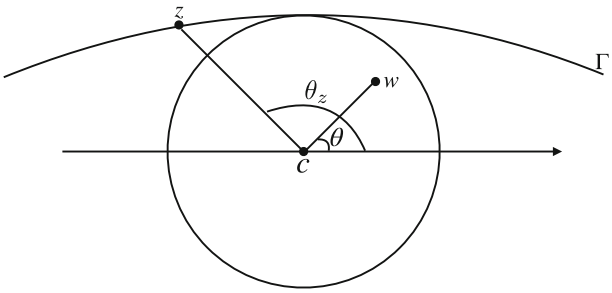

Fig. 1 Notation for the QBX method: Γ is the boundary, c is the center of expansion, w is the target point, z is a point on Γ, θ_z is the angle of $z-c$ measured from the x-axis, and θ is the angle of $w-c$ measured from the x-axis

$$\alpha_n = \frac{\mathrm{i}}{4}\int_\Gamma \frac{\partial}{\partial \mathbf{n}_z} H_n^{(1)}(k|z-c|)e^{\mathrm{i}n\theta_z}\psi(z)\mathrm{d}z \text{ for the double layer potentials,}$$

θ and θ_z are the polar angles of $w-c$ and $z-c$, respectively (See Fig. 1), and J_n and $H_n^{(1)}$ are the n^{th} order Bessel and Hankel functions of the first kind, respectively. The value of the layer potential at a point reasonably close to c is then approximated by the value of a partial wave expansion. Equation (3) is a direct consequence of applying Graf's addition theorem [13] to the Hankel function, and is the foundation of the fast multipole method (FMM) for the Helmholtz equation [14, 15]. The QBX scheme has been successfully combined with the FMM in [16] for solving the integral equation reformulation of PDEs.

This paper presents a new representation of local layer potential that uses complex local Taylor expansions and plane wave expansions rather than a classical numerical quadrature:

$$\phi(w) = \sum_{n=0}^{N} c_n (w-c)^n - 2\pi\mathrm{i}\left(\sum_{p=0}^{P}\sum_{j=1}^{J_u}\frac{b_p e^{\mathrm{i}p\pi r_j^u}}{1+\mathrm{i}s'(r_j^u)} - \sum_{p=-P}^{-1}\sum_{j=1}^{J_d}\frac{b_p e^{\mathrm{i}p\pi r_j^d}}{1+\mathrm{i}s'(r_j^d)}\right), \quad (4)$$

where the boundary Γ is defined by the parametric curve $z(t) = t + \mathrm{i}s(t)$, $s(t)$ is a real-coefficient polynomial for $t \in [-1, 1]$, $w = x + \mathrm{i}y$ is a target point, c is the center of the complex Taylor expansion, c_n and b_p are the complex coefficients of the Taylor expansion and plane wave type expansion, respectively, and $\{r_j^u\}_{j=1}^{J_u}$ and $\{r_j^d\}_{j=1}^{J_d}$ are the roots of the polynomial equation $w-(z+\mathrm{i}s(z)) = 0$ in the upper and lower complex half-plane, respectively. We refer to this new representation as the Quadrature by Two Expansions (QB2X). As the representation can be evaluated at any point in the box, the numerical scheme belongs to the class of QBX. Thus, we present the QB2X as an extension of the QBX and show their properties when both are used with a single expansion center for an entire FMM-leaf box. In linear algebra and harmonics analysis, the redundant basis sets (polynomial basis and exponential functions are linearly dependent) form a frame [17–19]. QB2X follows standard FMM error analysis and the number of QB2X expansion terms can be explicitly determined by the degree of the polynomial $s(t)$ and number of terms in the Fourier extension approximation of the density function. Numerical results in Sect. 3 show that for high order discretization of the boundary and oscillatory density functions, the QB2X method for Helmholtz layer potentials (QB2X-Helmholtz) converges rapidly and stably in the entire leaf box in the FMM tree structure.

In Eq. (4), instead of a partial wave expansion for the Helmholtz equation, we use the polynomial expansion $\sum_{n=0}^{N} c_n(w-c)^n$ which only satisfies the Laplace equation for w. There are two reasons for this particular choice of basis function. First, the logarithmic singularity of the Helmholtz Green's function can be explicitly extracted out [20], and one can directly apply the existing QB2X result for the Laplace equation (QB2X-Laplace) [21] which is based on contour integration and the residue theorem. The remaining formulation consists of the analytical part of the Helmholtz kernel which depends on the target point, source points, and density. They can be represented by a Fourier extension representation. Here, one of the major differences between QB2X-Helmholtz and QB2X-Laplace is that the Fourier extensions of analytical part of the Helmholtz kernel must be computed at every target point. Alternatively, one can use a two-dimensional (2D) Fourier extension [22] to avoid on-the-fly computation of one-dimensional (1D) Fourier extensions. Second, the numerical evaluation of a polynomial function is more efficient than that of the special Bessel or Hankel function. Note that the FMM handles the far-field layer potentials using the multipole and local expansions based on the low-rank properties derived from the separation of variables of the kernel function. The near-field singular or near-singular layer potential evaluation is therefore only required for the low- to moderate-frequency regimes when following the rule of "10 points per wavelength" in the numerical discretization. In this case, we expect there is no significant difference between the numbers of terms in the polynomial and partial wave expansions.

We organize this paper as follows: In Sect. 2, we present the derivation of the QB2X representation for the Helmholtz single layer potential. We omit the details for the double layer potential as the analysis is nearly identical to that of the single layer case. In Sect. 3, numerical results are presented to demonstrate the effectiveness of the QB2X representation using a single expansion center for each FMM-leaf box. We conclude the paper in Sect. 4 with a summary and discussions of future work.

2 Quadrature by Two Expansions for Helmholtz Layer Potentials

In this section, we first show the parametrization of the single and double layer potentials, and analytically extract the logarithmic singularity from the Helmholtz kernel to allow for the easy adoption of existing QB2X-Laplace analysis results. Next, the QB2X-Helmholtz representations are derived for both straight line and curved boundaries. Finally, we present a stable numerical scheme for the case when the roots of the denominator are close to each other.

2.1 Parametrization of Helmholtz Layer Potentials

Let the boundary Γ be parametrized by $z(t) = t + \mathrm{i}s(t)$, for $-1 \le t \le 1$, where $s(t)$ is a real-coefficient polynomial satisfying $s(0) = 0$, $s'(0) = 0$ after the proper rotations and translations. The single and double layer potentials at the target point $w = x + \mathrm{i}y$ are then parameterized as

$$S\psi(w) = \int_{-1}^{1} M(w,t)\psi(t)dt \text{ and } D\psi(w) = \int_{-1}^{1} L(w,t)\psi(t)dt, \tag{5}$$

where

$$\begin{aligned} M(w,t) &= \frac{\mathrm{i}}{4} H_0^{(1)}(kr(w,t))|z'(t)|, \\ L(w,t) &= -\frac{\mathrm{i}k}{4} \frac{(x-t)s'(t)-(y-s(t))}{r(w,t)} H_1^{(1)}(kr(w,t)), \\ r(w,t) &= \sqrt{(x-t)^2+(y-s(t))^2}, \\ |z'(t)| &= \sqrt{1+s'(t)^2}. \end{aligned} \tag{6}$$

Far-field layer potentials can be evaluated by standard multipole and local expansions, with their operations embedded within the FMM algorithm itself. Therefore, those evaluations are omitted here and we focus only on the evaluation of layer potentials in the near-field direct interactions between the leaf node and its neighbors (including itself) in the FMM algorithm (see Fig. 1 of [21]). We apply the series expansions of the second kind Bessel function (See [20, 23]), and explicitly extract the logarithmic singularity of $M(w,t)$ and $L(w,t)$ as

$$\begin{aligned} M(w,t) &= M_1(w,t)\ln\left((x-t)^2+(y-s(t))^2\right)+M_2(w,t), \\ L(w,t) &= L_1(w,t)\ln\left((x-t)^2+(y-s(t))^2\right)+L_2(w,t), \end{aligned} \tag{7}$$

where

$$\begin{aligned} M_1(w,t) &= -\frac{1}{4\pi} J_0(kr(w,t))|z'(t)|, \\ M_2(w,t) &= M(w,t) - M_1(w,t)\ln\left((x-t)^2+(y-s(t))^2\right), \\ L_1(w,t) &= \frac{k}{4\pi}((x-t)s'(t)-(y-s(t)))\frac{J_1(kr(w,t))}{r(w,t)}, \\ L_2(w,t) &= L(w,t) - L_1(w,t)\ln\left((x-t)^2+(y-s(t))^2\right). \end{aligned} \tag{8}$$

Consequently, M_1, M_2, L_1, and L_2 are analytic functions.

In this section, we focus on the single layer potential expressed as

$$S\psi(w) = \int_{-1}^{1} \ln\left((x-t)^2+(y-s(t))^2\right)\rho(w,t)dt + \int_{-1}^{1} M_2(w,t)\psi(t)dt, \tag{9}$$

where $\rho(w,t) = M_1(w,t)\psi(t)$. For each fixed target point w, $\rho(w,t)$ becomes a function purely of t. Thus, we can apply the well-developed 1D Fourier extension technique [24–26] to $\rho(w,t)$ to get

$$\rho(w,t) \approx \sum_{p=-P}^{P} a_p e^{\frac{\mathrm{i}p\pi}{2}t}, \tag{10}$$

where $a_p(w)$ can be computed by solving an optimization problem for each target point w. The optimization problem is usually exponentially ill-conditioned; however, the ill-conditioning can be resolved using the regularization technique described in [26, 27]. Similar to the QB2X-Laplace technique [21], we avoid the branch cut of the complex logarithmic function by using integration by parts to rewrite the single layer potential as

$$\begin{aligned} S\psi(w) = &\left[\ln\left((x-t)^2+(y-s(t))^2\right)f(t)\right]_{t=-1}^{t=1} \\ &+ 2\int_{-1}^{1} \frac{(x-t)+(y-s(t))s'(t)}{(x-t)^2+(y-s(t))^2} f(t)dt + \int_{-1}^{1} M_2(w,t)\psi(t)dt, \end{aligned} \tag{11}$$

where $f(t)$ is the antiderivative of $\rho(w,t)$ given by

$$f(t) = \sum_{\substack{p=-P \\ p\neq 0}}^{P} \frac{2a_p}{\mathrm{i}p\pi} e^{\frac{\mathrm{i}p\pi}{2}t} + a_0 t \tag{12}$$

for the given target point w. $f(t)$ can be further simplified by reapplying the Fourier extension (or applying a precomputed mapping from polynomial basis to Fourier series) to the term $a_0 t$ to get

$$f(t) = \sum_{p=-P}^{P} b_p e^{\frac{\mathrm{i}p\pi}{2}t}. \tag{13}$$

In Eq. (11), the first term can be evaluated directly. The integrand in the last term is a smooth analytic function of t and can be accurately and efficiently evaluated using any standard quadrature rules. We focus on the numerical evaluation of the second term which contains the singular or near singular component of the kernel, and rewrite the integral in the complex form as

$$\begin{aligned} &2\int_{-1}^{1} \frac{(x-t)f(t) + (y-s(t))s'(t)f(t)}{(x-t)^2 + (y-s(t))^2}\mathrm{d}t \\ &= \left(\int_{-1}^{1} \frac{f(t)}{w-(t+\mathrm{i}s(t))}\mathrm{d}t + \int_{-1}^{1} \frac{f(t)}{w^*-(t-\mathrm{i}s(t))}\mathrm{d}t\right) \\ &\quad + \mathrm{i}\left(\int_{-1}^{1} \frac{s'(t)f(t)}{w-(t+\mathrm{i}s(t))}\mathrm{d}t - \int_{-1}^{1} \frac{s'(t)f(t)}{w^*-(t-\mathrm{i}s(t))}\mathrm{d}t\right), \end{aligned} \tag{14}$$

where $w = x + \mathrm{i}y$ and $w^* = x - \mathrm{i}y$. We omit the details for the double layer potential as it can be simplified in an identical manner by replacing M_1 and M_2 by L_1 and L_2 in Eq. (9), respectively. Note that Eq. (14) is now similar to the layer potentials for the Laplace equation (e.g., see Eq. (6) in [21]). Therefore, results from QB2X-Laplace can be adopted to derive the QB2X-Helmholtz representations.

2.2 QB2X-Helmholtz

The derivation of QB2X-Helmholtz for Eq. (14) follows the same procedure as QB2X-Laplace [21]. First, the numerator function is replaced by its Fourier extension. Then, the sum is separated into integrals of non-negative and negative Fourier modes. Each integral from -1 to 1 is represented by the integrals over the other segments using the residue theorem (See contours presented in Figs. 2 and 3). Finally, by introducing the center of expansion c, the QB2X-Helmholtz representation is derived. A more detailed derivation can be found in Ref. [21]. Therefore, we omit the derivation and present the final QB2X-Helmholtz representations for the flat and curved boundary cases.

For a boundary curve $s(t) = 0$ (flat boundary), by substituting the Fourier extension of f and separating the sum by non-negative and negative modes, the first two integrals in Eq. (14) become complex integrals on the line segment from -1 to 1 on the complex plane, both

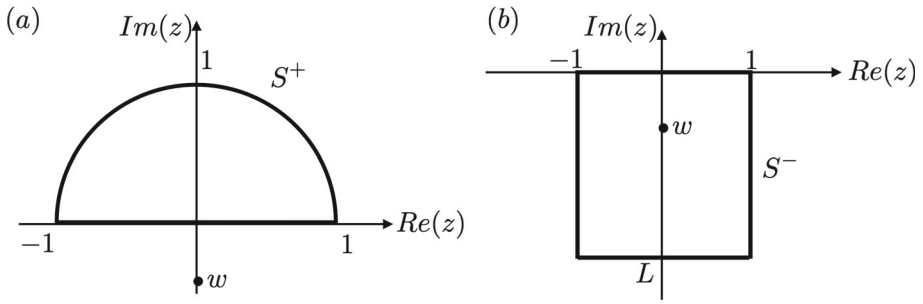

Fig. 2 Straight line boundary: **a** Contour C_1 for I_1 **b** Contour C_2 for I_2

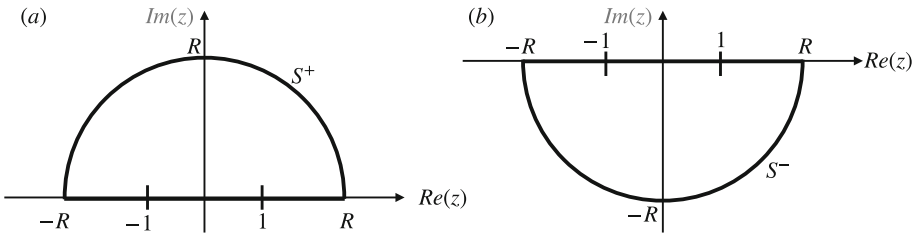

Fig. 3 Curved boundary: **a** C_1 contour for I_1 and **b** C_2 contour for I_2

with the form of

$$\int_{-1}^{1} \frac{f(z)}{w-z}\mathrm{d}z \approx \underbrace{\sum_{p=0}^{P} \int_{-1}^{1} \frac{b_p e^{\frac{ip\pi}{2}z}}{w-z}\mathrm{d}z}_{=I_1} + \underbrace{\sum_{p=-P}^{-1} \int_{-1}^{1} \frac{b_p e^{\frac{ip\pi}{2}z}}{w-z}\mathrm{d}z}_{=I_2}. \tag{15}$$

Using the contours proposed in Fig. 2 along with the residue theorem, we can represent this approximation in QB2X as the sum of a polynomial expansion and a plane wave type expansion

$$\int_{-1}^{1} \frac{f(z)}{w-z}\mathrm{d}z \approx \sum_{n=0}^{N} c_n (w-c)^n + 2\pi \mathrm{i} \sum_{p=-P}^{-1} b_p e^{\frac{\mathrm{i}p\pi}{2}w}, \tag{16}$$

where c is the center of the polynomial expansion, b_p is the Fourier coefficients in Eq. (13), and

$$c_n = \sum_{p=0}^{P} \int_{S^+} \frac{b_p e^{\frac{\mathrm{i}p\pi}{2}z}}{(z-c)^{n+1}}\mathrm{d}z + \sum_{p=-P}^{-1} \int_{S^-} \frac{b_p e^{\frac{\mathrm{i}p\pi}{2}z}}{(z-c)^{n+1}}\mathrm{d}z. \tag{17}$$

Unlike the order of convergence concept from classical quadrature rules, the QB2X scheme evaluates the integral in Eq. (15) using a truncated analytical formula which allows for forward error analysis. The error sources include the approximation of the Helmholtz Green's function in the low-frequency regime (∼10 points per wavelength) with its Laplace counterpart (plus smooth function corrections), discretization errors from the boundary geometry and density function, accuracy of the Fourier extension, and truncation of the polynomial expansion in Eq. (16). As in classical numerical analysis, the errors from the kernel, geometry, and density approximations can be studied by inspecting the decay rate of the corresponding expansion

coefficients. Since the source points on the segments S^+ and S^- are well-separated from the target point w, which is the only pole in the integrand, standard FMM error analysis can be applied to determine the necessary number of terms in the polynomial expansion. As shown in Sect. 3, for a prescribed accuracy requirement, the number of polynomial expansion terms needed is approximately the same as those from the worst-case FMM analysis for the Laplace kernel, i.e., $N = 9$ for 3-digit, $N = 18$ for 6-digit, $N = 27$ for 9-digit, and $N = 36$ for 12-digit accuracy.

When the boundary curve $s(t)$ is not flat or nearly-flat, one main challenge for the QBX representation when used as a single expansion for the entire FMM-leaf box is the slow convergence of the partial wave or polynomial expansions. This is demonstrated numerically in Sect. 3. The QB2X-Helmholtz representation for a curved boundary which converges rapidly inside the entire FMM-leaf box is presented here. We focus on the singular or nearly-singular parts of the Helmholtz layer potentials given by Eq. (14) in the complex form

$$\begin{aligned}&\int_{-1}^{1} \frac{f(z)}{w-(z+\mathrm{i}s(z))}\mathrm{d}z \\ &\approx \underbrace{\sum_{p=0}^{P}\int_{-1}^{1} \frac{b_p e^{\frac{ip\pi}{2}z}}{w-(z+\mathrm{i}s(z))}\mathrm{d}z}_{=I_1} + \underbrace{\sum_{p=-P}^{-1}\int_{-1}^{1} \frac{b_p e^{\frac{ip\pi}{2}z}}{w-(z+\mathrm{i}s(z))}\mathrm{d}z}_{=I_2}.\end{aligned} \tag{18}$$

Again, derivation follows the same procedure with QB2X-Laplace [21]. Based on the contours in Fig. 3 and residue theorem, the integral in (18) can be approximated by

$$\begin{aligned}&\int_{-1}^{1} \frac{f(z)}{w-(z+\mathrm{i}s(z))}\mathrm{d}z \\ &\approx \sum_{n=0}^{N} c_n (w-c)^n - 2\pi\mathrm{i}\left(\sum_{p=0}^{P}\sum_{j=1}^{J_u} \frac{b_p e^{\frac{ip\pi}{2}r_j^u}}{1+\mathrm{i}s'(r_j^u)} - \sum_{p=-P}^{-1}\sum_{j=1}^{J_d} \frac{b_p e^{\frac{ip\pi}{2}r_j^d}}{1+\mathrm{i}s'(r_j^d)}\right),\end{aligned} \tag{19}$$

where c is the center of the polynomial expansion, b_p is the Fourier coefficients in Eq. (13), $\{r_j^u\}_{j=1}^{J_u}$ and $\{r_j^d\}_{j=1}^{J_d}$ are the roots of $w-(z+\mathrm{i}s(z))=0$ in the upper and lower half planes, respectively, and

$$c_n = \sum_{p=-P}^{P} b_p \left(\int_{1}^{\infty} \frac{e^{\frac{ip\pi}{2}z}}{(z+\mathrm{i}s(z)-c)^{n+1}}\mathrm{d}z + \int_{-\infty}^{-1} \frac{e^{\frac{ip\pi}{2}z}}{(z+\mathrm{i}s(z)-c)^{n+1}}\mathrm{d}z\right). \tag{20}$$

Each singular or nearly-singular term of the Helmholtz layer potential in Eq. (14) can be computed by directly applying Eq. (19). Note that the integrals composing c_n can be computed utilizing the special exponential integral function defined by $E_n(z) = z^{n-1}\int_z^\infty e^{-t}t^{-n}\mathrm{d}t$ [28, 29]. Moreover, since they are independent of target points, these integrals are only computed once for each FMM-leaf box and stored in a two dimensional table for different p and n values. This table is then used for all target points. Instead of a polynomial expansion in Eq. (19), it may be possible to use a partial wave expansion for the Helmholtz equation. However, since polynomial expansion evaluations are computationally cheaper than partial wave expansions based on the special function, we choose to use the Laplacian kernel and polynomial expansions. It is important to understand the trade-off in QB2X between computational cost and resulting accuracy. QB2X allows for higher-order discretization but requires more operations. However these additional operations are "local" (i.e., requiring no

communication between leaf boxes) in the computer system and are highly parallelizable. We refer interested readers to ExaFMM [30] for discussions of the polynomial basis and parallelization techniques.

Remark As noted in QB2X-Laplace, when some of the roots of the polynomial equation $w-(z+\mathrm{i}s(z))=0$ are close to each other in rare cases, the computation of the residues (plane wave type expansion) may experience a loss of significance due to the subtraction of two close numbers. For example, consider a third degree polynomial $s(z)$ with leading coefficient c_0, and assume the denominator $(w-(z+\mathrm{i}s(z)))=0$ has three roots: r_1, r_2 in the upper complex half-plane that are very close to each other, and r_3 in the lower complex half-plane. Then the plane wave type expansion from the residue theorem becomes

$$\begin{aligned}&\frac{1}{2\pi\mathrm{i}}\int_{C_1}\frac{b_p e^{\frac{\mathrm{i}p\pi}{2}z}}{c_0(z-r_1)(z-r_2)(z-r_3)}\mathrm{d}z\\&=\frac{b_p e^{\frac{\mathrm{i}p\pi}{2}r_1}}{c_0(r_1-r_2)(r_1-r_3)}+\frac{b_p e^{\frac{\mathrm{i}p\pi}{2}r_2}}{c_0(r_2-r_1)(r_2-r_3)},\end{aligned}\tag{21}$$

where C_1 is the contour given in Fig. 3a. Equation (21) clearly shows the loss of accuracy when roots are close to each other. Following the idea from QB2X-Laplace, it can be computed stably using

$$\int_{C_1}\frac{b_p e^{\frac{\mathrm{i}p\pi}{2}z}}{c_0(z-r_1)(z-r_2)(z-r_3)}\mathrm{d}z\approx\frac{2\pi\mathrm{i}b_p}{c_0}\sum_{m=1}^{M}\delta_{m-1}\left(\frac{e^{\frac{\mathrm{i}p\pi}{2}z}}{z-r_3}\right)^{(m)}\Bigg|_{z=r_c}.\tag{22}$$

where r_c is the midpoint between r_1 and r_2 and δ_{m-1} is coefficients of the product of the geometric series of $1/(1-\frac{r_1-r_c}{z-r_c})$ and $1/(1-\frac{r_2-r_c}{z-r_c})$. Since the geometric series decays rapidly, only a small number of terms is required in this alternative representation for cases when roots are close to each other. We present comparisons of the original plane wave type formula in Eq. (21) with the alternative representation in Eq. (22) for a curved boundary given by $s(z)=-\left(\frac{4\times10^{19}}{-8.7\times10^{19}+\pi^2}\right)z^3+\left(\frac{-6.3\times10^{19}+\pi^2}{-8.7\times10^{19}+\pi^2}\right)z^2$ and $w=\left(\frac{3}{5}+\frac{29}{100}\mathrm{i}\right)+\frac{\mathrm{i}\pi^2}{10^{20}}+\frac{4.48\times10^{19}+6.4\times10^{19}\mathrm{i}}{-8.7\times10^{19}+\pi^2}$. Three roots of $w-(z+\mathrm{i}s(z))=0$ are $r_1=\frac{1}{5}-\pi\times10^{-10}+\frac{1}{2}\mathrm{i}$, $r_2=\frac{1}{5}+\pi\times10^{-10}+\frac{1}{2}\mathrm{i}$, and $r_3=\frac{-7.8\times10^{19}+\pi^2}{4\times10^{19}}-\mathrm{i}$. We construct the Helmholtz layer potential using $p=1$ and $b_p=1$. Integration over C_1 using the residue theorem in Eq. (21) yields a result of $0.6757127940654755-0.07931315898895264\mathrm{i}$ and the new representation in Eq. (22) with $M=3$ yields $0.67571272714158517293-0.07931328249252365183\mathrm{i}$. Equation (21) is evaluated using `NIntegrate` command with a precision goal of 24 digits in Mathematica as the reference solution. Compared with the reference solution, the absolute error of the direct residue theorem is 1.4×10^{-7}, and it becomes 4.6×10^{-18} for the new representation. An additional example with a fourth degree polynomial can be found in [21]. In a practical implementation such as Chunkie [31], each chunk of the boundary is resolved with low-degree polynomials (typically having degree less than 20). Because of this, stable computations require an additional polynomial root-finding algorithm along with a pairwise comparison of all complex roots, which introduces only minimal computational cost [32, 33]. These operations can be efficiently parallelized as they don't require communication between leaf boxes. Note that loss of accuracy does not happen in the case of second degree polynomials due to the symmetry of the two roots.

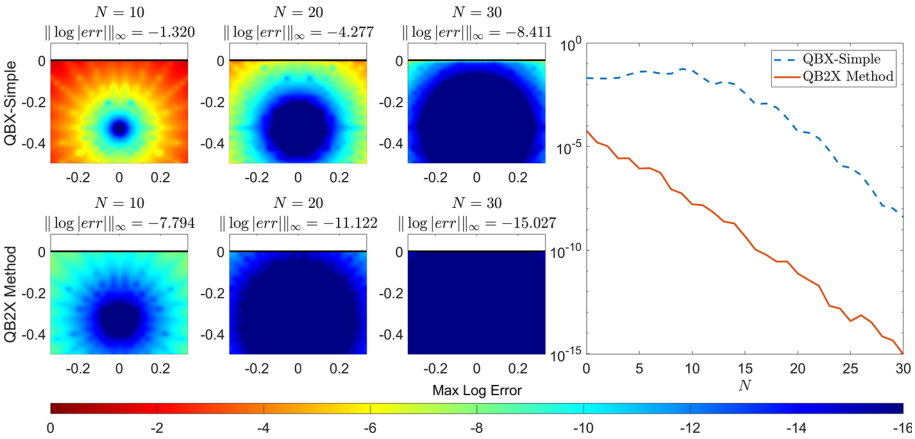

Fig. 4 Single layer potentials with center $c = -\frac{1}{3}\mathrm{i}$ for $s(t) = 0$, $-1 \le t \le 1$: (*Left*) Errors from both QBX-Simple (upper) and QB2X (lower) with respect to reference solutions for density function $\psi(t) = \cos(20t)$ with $P = 50$. (*Right*) Convergence of the L^∞ errors for both the QBX-Simple (dashed line) and QB2X (solid line) cases with respect to N

3 Numerical Results

In this section, we present numerical results to demonstrate the effectiveness of the QB2X technique for the Helmholtz layer potentials. Since QB2X provides a representation that is valid in the entire FMM-leaf box, we compare it with our own QBX implementation which also uses a single expansion for the same FMM-leaf box. This comparison is for illustrative purposes only, since it is recommended to use multiple expansion centers for QBX in a practical setting. For this reason, we refer to our simple implementation of QBX as QBX-Simple throughout this section so as not to be confused with the state-of-the-art QBX implementation. The boundary is given by the polynomial $s(t)$, $-1 \le t \le 1$, and the FMM-leaf box center is set on the imaginary axis at either $-\frac{1}{3}\mathrm{i}$ or $-\frac{1}{6}\mathrm{i}$. We test the accuracy of QB2X-Helmholtz for different P, N, and k values, where P is the number of terms used for the Fourier extensions, N is the number of terms in the complex Taylor expansions, and k is the wave number. In this paper, we restrict our attention only to k values for low- to moderate-frequencies which is required when evaluating the local direct interactions in the FMM algorithm. We compute reference solutions using the `NIntegrate` command from Mathematica with a precision goal of 24 digits for all numerical examples. We use the L^∞ norm when comparing QB2X or QBX-Simple solutions to the reference solutions, and present the number of digits in the error analysis computed using $\| \log |err| \|_\infty = \max_w \log \| Q\psi(w) - R\psi(w) \|$, where $Q\psi(w)$ is the QBX-Simple or QB2X solution and $R\psi(w)$ is the reference Helmholtz single layer or double layer solution.

In the first example, we show the QBX-Simple representation with the QB2X-Helmholtz representation for a flat boundary $s(t) = 0$ with a mildly oscillating trigonometric density function $\psi(t) = \cos(20t)$. We set $P = 50$ and $k = 1$. Figure 4 shows the errors of both the QBX-Simple and QB2X methods for $N = 10$, 20 and 30 and the convergence for different N values. For this example, QB2X-Helmholtz reaches its asymptotic error minimum when $N = 31$, and $\| \log |err| \|_\infty = -15.033$ which is approximately machine precision.

When the boundary is a straight line segment, we noticed that the convergence of QBX-Simple depends on the periodicity (frequency) of the density function. For low-frequency

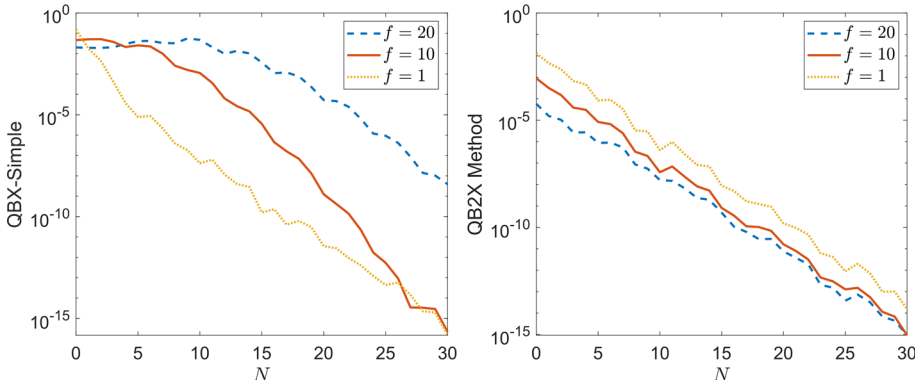

Fig. 5 Single layer potentials with center $c = -\frac{1}{3}\mathrm{i}$ for $s(t) = 0$, $-1 \le t \le 1$: (*Left*) QBX-Simple and (*Right*) QB2X convergence for density function $\psi(t) = \cos(ft)$ with f=1 (dotted line), 10 (solid line), 20 (dashed line) and increasing N values. We set $P = 50$

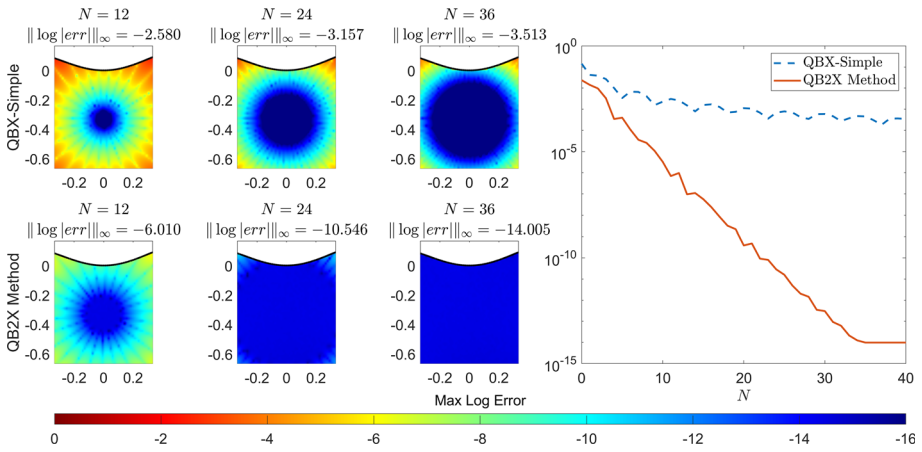

Fig. 6 Single layer potentials with center $c = -\frac{1}{3}\mathrm{i}$ for $s(t) = t^2 + \frac{t^3}{10} - 2t^4$, $-1 \le t \le 1$: (*Left*) Errors from QBX-Simple (upper) and QB2X (lower) for density function $\psi(t) = 1$ with $P = 100$. (*Right*) Convergence of the L^∞ error in QBX-Simple (dashed line) and QB2X (solid line) for increasing N values

density functions, both QBX-Simple and QB2X-Helmholtz work well. However as the frequency of the density function increases, the performance of QBX-Simple deteriorates rapidly. On the other hand, the error in QB2X follows the standard FMM error analysis and the convergence (with respect to N) is nearly independent of the frequency of the density function. This is demonstrated in Fig. 5 for different frequencies f in the density function $\psi(t) = \cos(ft)$.

In the second example, we consider a non-flat boundary given by $s(t) = t^2 + \frac{t^3}{10} - 2t^4$. We focus on the nonlinear contribution from the boundary geometry and set the density function to the constant function $\psi(t) = 1$ and $k = 1$. In the left of Fig. 6, we show the error for $N = 12$, 24, and 36. For the QBX-Simple representation centered at $(0, -\frac{1}{3})$, although the L^∞ error is small close to the center, the error close to the boundary and the FMM-leaf box edges decays very slowly when N increases. On the other hand, the QB2X representation achieves machine precision accuracy at all points in the FMM-leaf box when $N = 36$. In

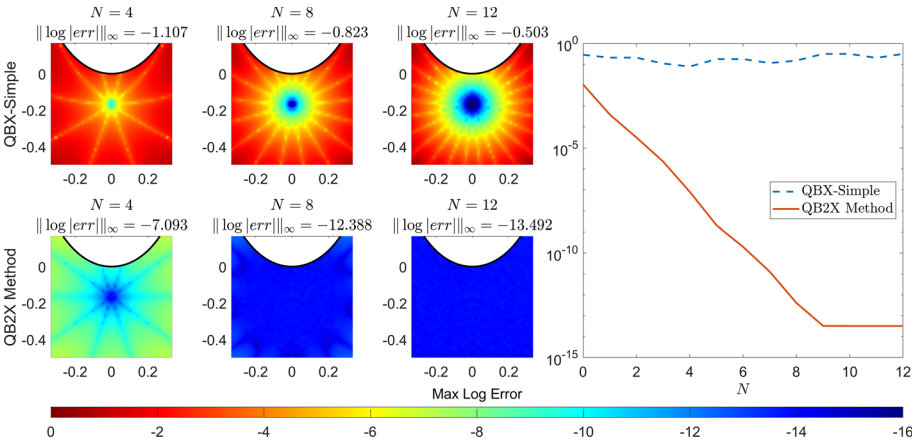

Fig. 7 Single layer potentials with center $c = -\frac{1}{6}\mathrm{i}$ for $s(t) = 5t^4 + 2t^2$, $-1 \le t \le 1$: (*Left*) Errors from QBX-Simple and QB2X for $\psi(t) = 1$, $N = 4$, 8, 12, and $P = 100$. (*Right*) L^∞ error convergence for both QBX-Simple (dashed line) and QB2X (solid line) for increasing N values

the right of Fig. 6, we plot the convergence of QBX-Simple and QB2X as a function of N. The convergence of QB2X follows the standard FMM error analysis and reaches machine precision when $N \approx 36$. The QBX-Simple representation is unable to effectively resolve the nonlinearity from the curved boundary and the error decays slowly. In both cases, $P = 100$ is used in the Fourier extension to guarantee machine precision accuracy.

In order to further demonstrate the convergence of the QBX-Simple and QB2X representations and their dependency on the boundary geometry, in the third example, we consider the boundary setting $s(t) = 5t^4 + 2t^2$ which curves rapidly away from the partial wave (QBX) or polynomial (QB2X) expansion center. This extreme geometry setting should never happen in a uniform FMM tree structure but may appear when an adaptive FMM tree is used to more effectively resolve the solution. All the other features are the same as those in the previous example. On the left of Fig. 7, the error from QBX-Simple decays slowly in most of the computational domain. Since all expansion coefficients are computed with machine precision, the slow convergence of QBX-Simple is due to the truncation of the expansion. Clearly more expansion terms are required when the boundary is not nearly-flat. On the other hand, the QB2X representation allows for a high degree polynomial description of the boundary, and the error in this example converges to approximately machine precision when $N = 9$. On the right of Fig. 7, we present the L^∞ error convergence for both representations. Clearly, the convergence of QB2X follows the standard FMM error analysis. For the particular geometry setting, as the FMM-leaf box size is $\frac{2}{3} \times \frac{2}{3}$, we have $\|w - c\| \le \frac{\sqrt{2}}{3}$, and for $z \in [-\infty, -1] \cup [1, \infty]$, $\|z + \mathrm{i}s(z)\epsilon c\| \ge \sqrt{(\pm 1 - 0)^2 + (s(\pm 1) + \frac{1}{6})^2}$. Therefore the local polynomial expansion converges like $\left(\frac{\|w-c\|}{\|z+\mathrm{i}s(z)-c\|}\right)^N \approx 0.06567^N$. Applying this worst case analysis, when $N = 12$, $0.06567^{12} \approx 6.43 \times 10^{-15}$, QB2X should achieve machine precision accuracy. This analysis is consistent with the numerical results.

In many existing implementations of the boundary integral equation method, the density functions are usually approximated by piecewise polynomials (instead of a Fourier series). We therefore consider a polynomial density function $\psi(t) = \frac{2t^2+2t+3}{4}$ in the next example and show the performance of QB2X. In Fig. 8, we show the errors for $N = 6$, 12, 18, 24,

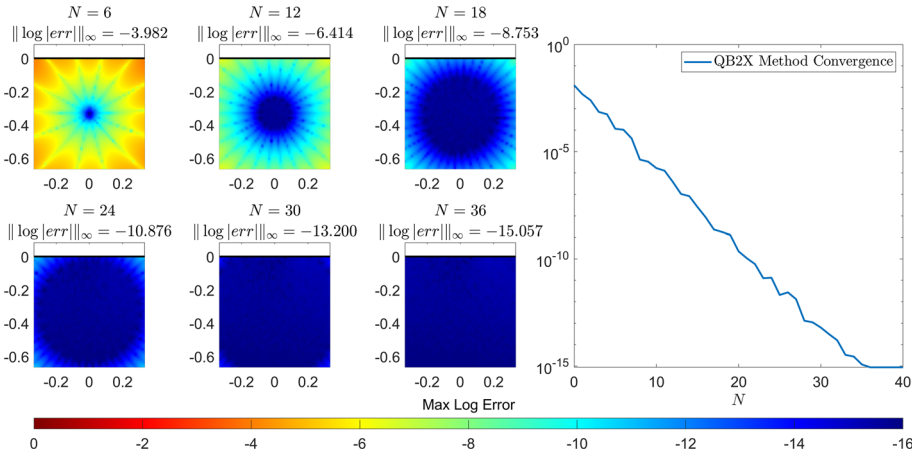

Fig. 8 Single layer potentials with center $c = -\frac{1}{3}\mathrm{i}$ for $s(t) = 0$, and $\psi(t) = \frac{2t^2+2t+3}{4}$, $-1 \le t \le 1$. $P = 50$: (*Left*) QB2X errors for $N = 6$, 12, 18, 24, 30, and 36. $P = 50$. (*Right*) Convergence of the L^∞ error for different N values

30, and 36 and convergence of the QB2X method for a flat boundary. We set $P = 50$ and $k = 1$. The numerical results show that QB2X reaches machine precision accuracy at about $N = 36$ where $\| \log |err| \|_\infty = -15.0575$.

There are at least two ways to derive the Fourier series required in the QB2X method, by applying existing Fourier extension algorithms on the fly, or first representing the density functions as piecewise polynomials, and then map the polynomials to Fourier series using precomputed (using Fourier extension) transformation tables from the polynomial basis to Fourier basis. The latter technique can be more efficient but requires additional storage.

In the FMM algorithm, the evaluation of the singular and nearly-singular Helmholtz layer potentials is only required in the local direct interactions of the leaf boxes of the FMM tree structure. Therefore, we only need to consider low- to moderate-frequency k values. In the next example, we consider the curved boundary $s(t) = 5t^4 + 2t^2$ and density function $\psi(t) = 1$ for wave numbers $k = 1$ and $k = 10$. Clearly, for larger k value, more Fourier extension terms are required to capture the linear and nonlinear contributions. We set $P = 100$ for $k = 1$ and $P = 300$ for $k = 10$. On the left of Fig. 9, we show the error results for $N = 4, 8$, and 12 and different k values. On the right, we show the convergence of the QB2X-Helmholtz method as N increases. The numerical results show that when a sufficient number of Fourier series terms are used, the convergence properties for $k = 1$ and $k = 10$ as a function of N are at similar rates, and reach machine precision for all target points inside the FMM leaf box.

Finally, we show the QB2X performance for the double layer Helmholtz potentials. We found that the numerical results for double layer potentials are similar to those for single layer potentials. In Fig. 10, we set all the parameters the same as those in Fig. 8 ($s(t) = 0$, $k = 1$, and $\psi(t) = \frac{2t^2+2t+3}{4}$) and compute the double layer potential using QB2X-Helmholtz. Both the error distributions and convergence rates are similar to the single layer case. In Fig. 11, we use the same settings as in Fig. 6 ($s(t) = t^2 + \frac{t^3}{10} - 2t^4$, $k = 1$, $\psi(t) = 1$) and compute the double layer Helmholtz potential using both the QBX-Simple and QB2X-Helmholtz methods. Clearly, each method shows similar error behavior and rate of convergence (L^∞ norm) for single and double layer potentials.

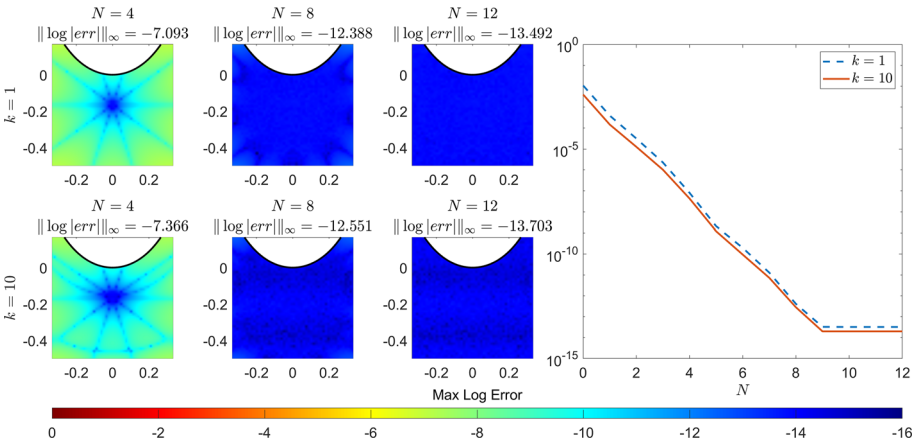

Fig. 9 Single layer potentials with center $c = -\frac{1}{6}\mathrm{i}$ for $s(t) = 2t^2 + 5t^4$ and $\psi(t) = 1$, $-1 \le t \le 1$: (*Left*) QB2X errors for wave numbers $k = 1$ with $P = 100$ (upper), and for $k = 10$ with $P = 300$ (lower) when $N = 4$, 8, and 12. (*Right*) QB2X convergence (L^∞ error) as a function of N for $k = 1$ (dashed line) and $k = 10$ (solid line)

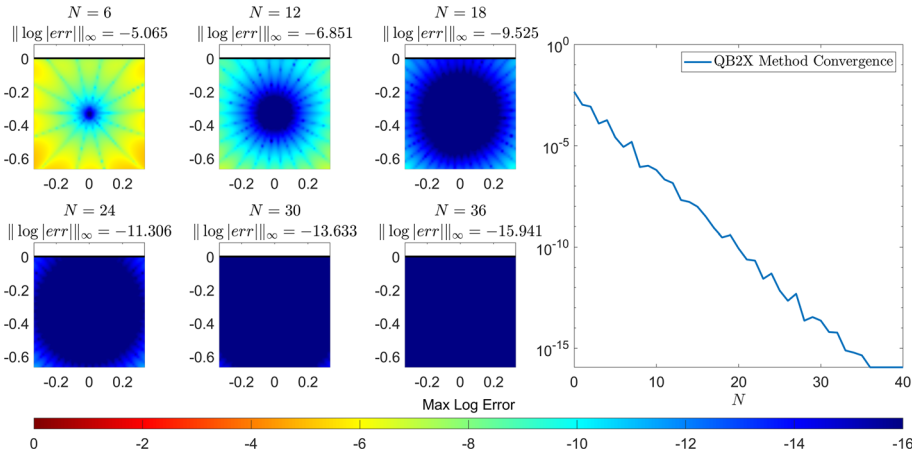

Fig. 10 Double layer potential with center $c = -\frac{1}{3}\mathrm{i}$ for $s(t) = 0$ and $\psi(t) = \frac{2t^2+2t+3}{4}$, $-1 \le t \le 1$. $k = 1$: (*Left*) QB2X errors for $N = 6$, 12, 18, 24, 30, and 36. We set $P = 50$. (*Right*) Convergence of the L^∞ error for different N values

4 Conclusions

The main contribution of this paper is a new QB2X representation for evaluating the Helmholtz single and double layer potentials in two-dimensional space. The QB2X-Helmholtz method uses both local complex Taylor expansions and plane wave type expansions to effectively capture the nonlinear contributions from the boundary geometry. Under minor restrictions on the discretization of the boundary geometry, the QB2X-Helmholtz representation can be valid and accurate in the entire leaf box of the FMM hierarchical tree structure, where the adaptive tree structures only depend on the discretization error from the density function and boundary geometry. Nonlinear contributions from the boundary geometry becomes analytically embedded within the exponential expansions.

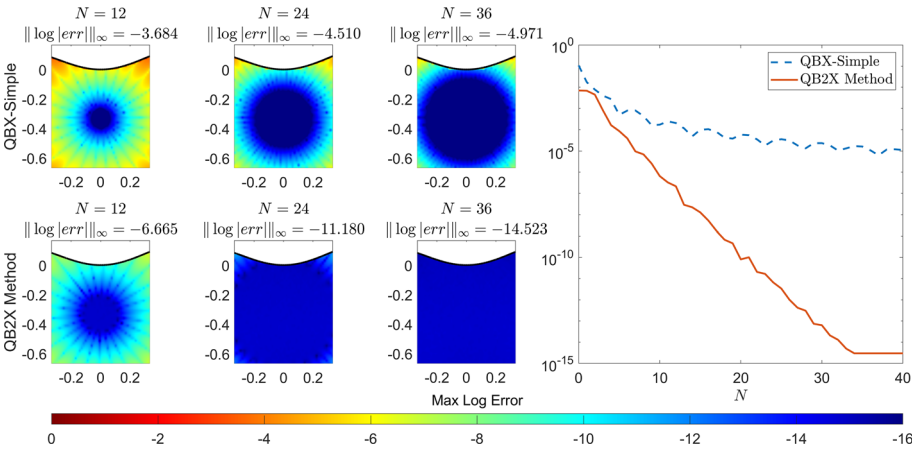

Fig. 11 Double layer potentials with center $c = -\frac{1}{3}\mathrm{i}$ for $s(t) = t^2 + \frac{t^3}{10} - 2t^4$ and $\psi(t) = 1$, $-1 \le t \le 1$. $k = 1$: (*Left*) QBX-Simple (upper) and QB2X (lower) errors for different N values. We set $P = 100$. (*Right*) Convergence of the L^∞ error for both the QBX-Simple (dashed line) and QB2X (solid line) methods for increasing N

Preliminary numerical results show the excellent accuracy and stability properties of QB2X-Helmholtz. The extension of QB2X-Helmholtz to the modified Helmholtz (Yukawa) kernel [34] is straight forward and is being implemented. Extending the QB2X method to 3D layer potentials is challenging and is currently being studied. A more comprehensive comparison between QB2X and other quadrature rules such as QBX, adaptive, and global quadrature rules remains as future work and will be reported in a later publication.

Funding M.H. Cho was supported by NSF grant DMS 2012382 and a grant from the Simons Foundation (No. 404499). J. Huang was supported by NSF grant DMS 2012451.

Data Availability The datasets generated during and/or analyzed during the current study are available from the corresponding author on reasonable request.

Declarations

Competing Interests The authors have no relevant financial or non-financial interests to disclose.

References

1. Lewis, A., Taha, H., Strinkovski, A., Manevitch, A., Khatchatouriants, A., Dekhter, R., Ammann, E.: Near-field optics: from subwavelength illumination to nanometric shadowing. Nat. Biotechnol. **21**(11), 1378–1386 (2003)
2. Khattak, H.K., Bianucci, P., Slepkov, A.D.: Linking plasma formation in grapes to microwave resonances of aqueous dimers. Proc. Natl. Acad. Sci. **116**(10), 4000–4005 (2019)
3. Tsantili, I.C., Cho, M.H., Cai, W., Karniadakis, G.E.: A computational stochastic methodology for the design of random meta-materials under geometric constraints. SIAM J. Sci. Comput. **40**(2), B353–B378 (2018)
4. Alpert, B.K.: Hybrid gauss-trapezoidal quadrature rules. SIAM J. Sci. Comput. **20**(5), 1551–1584 (1999)
5. Kapur, S., Rokhlin, V.: High-order corrected trapezoidal quadrature rules for singular functions. SIAM J. Numer. Anal. **34**(4), 1331–1356 (1997)
6. Wu, B., Martinsson, P.G.: Zeta correction: a new approach to constructing corrected trapezoidal quadrature rules for singular integral operators. Adv. Comput. Math. **47**(3), 1–21 (2021)

7. Bremer, J., Gimbutas, Z., Rokhlin, V.: A nonlinear optimization procedure for generalized gaussian quadratures. SIAM J. Sci. Comput. **32**(4), 1761–1788 (2010)
8. Yarvin, N., Rokhlin, V.: Generalized gaussian quadratures and singular value decompositions of integral operators. SIAM J. Sci. Comput. **20**(2), 699–718 (1998)
9. Bruno, O.P., Kunyansky, L.A.: A fast, high-order algorithm for the solution of surface scattering problems: basic implementation, tests, and applications. J. Comput. Phys. **169**(1), 80–110 (2001)
10. Duffy, M.G.: Quadrature over a pyramid or cube of integrands with a singularity at a vertex. SIAM J. Numer. Anal. **19**(6), 1260–1262 (1982)
11. Beale, J.T., Lai, M.C.: A method for computing nearly singular integrals. SIAM J. Numer. Anal. **38**(6), 1902–1925 (2001)
12. Klöckner, A., Barnett, A., Greengard, L., O'Neil, M.: Quadrature by expansion: A new method for the evaluation of layer potentials. J. Comput. Phys. **252**, 332–349 (2013)
13. Abramowitz, M., Stegun, I.A.: Handbook of mathematical functions with formulas, graphs, and mathematical tables, vol. 55. US Government printing office (1964)
14. Cho, M.H., Cai, W.: A wideband fast multipole method for the two-dimensional complex helmholtz equation. Comput. Phys. Commun. **181**(12), 2086–2090 (2010)
15. Rokhlin, V.: Rapid solution of integral equations of scattering theory in two dimensions. J. Comput. Phys. **86**(2), 414–439 (1990)
16. Rachh, M., Klöckner, A., O'Neil, M.: Fast algorithms for quadrature by expansion i: globally valid expansions. J. Comput. Phys. **345**, 706–731 (2017)
17. Adcock, B., Huybrechs, D.: Frames and numerical approximation. SIAM Rev. **61**(3), 443–473 (2019)
18. Casazza, P.G., Kutyniok, G.: Finite Frames: Theory and Applications. Springer (2012)
19. Duffin, R.J., Schaeffer, A.C.: A class of nonharmonic fourier series. Trans. Am. Math. Soc. **72**(2), 341–366 (1952)
20. Colton, D.L., Kress, R., Kress, R.: Inverse acoustic and electromagnetic scattering theory, vol. 93. Springer (1998)
21. Ding, L., Huang, J., Marzuola, J.L., Tang, Z.: Quadrature by two expansions: Evaluating laplace layer potentials using complex polynomial and plane wave expansions. J. Comput. Phys. **428**, 109963 (2021)
22. Matthysen, R., Huybrechs, D.: Function approximation on arbitrary domains using fourier extension frames. SIAM J. Numer. Anal. **56**(3), 1360–1385 (2018)
23. Kress, R.: Linear Integral Equations, vol. 82. Springer Science & Business Media (2013)
24. Boyd, J.P.: A comparison of numerical algorithms for Fourier extension of the first, second, and third kinds. J. Comput. Phys. **178**(1), 118–160 (2002)
25. Bruno, O.P., Han, Y., Pohlman, M.M.: Accurate, high-order representation of complex three-dimensional surfaces via Fourier continuation analysis. J. Comput. Phys. **227**(2), 1094–1125 (2007)
26. Huybrechs, D.: On the fourier extension of nonperiodic functions. SIAM J. Numer. Anal. **47**(6), 4326–4355 (2010)
27. Barnett, A.H.: How exponentially ill-conditioned are contiguous submatrices of the Fourier matrix? SIAM Rev. **64**(1), 105–131 (2022)
28. Lozier, D.W.: Nist digital library of mathematical functions. Ann. Math. Artif. Intell. **38**, 105–119 (2003)
29. Olver, F., Lozier, D., Boisvert, R., Clark, C.: Digital library of mathematical functions: Online companion to nist handbook of mathematical functions (cup). National Insitute of Standards and Technology, Gaithersburg (2010)
30. Wang, T., Yokota, R., Barba, L.A.: ExaFMM: a high-performance fast multipole method library with C++ and python interfaces. J. Open Sour. Softw. **6**(61), 3145 (2021)
31. chunkie: a MATLAB integral equation toolbox. https://github.com/fastalgorithms/chunkie
32. Kim, M.H., Sutherland, S.: Polynomial root-finding algorithms and branched covers. SIAM J. Comput. **23**(2), 415–436 (1994)
33. Zeng, Z.: Algorithm 835: Multroot—a matlab package for computing polynomial roots and multiplicities. ACM Trans. Math. Softw. (TOMS) **30**(2), 218–236 (2004)
34. Huang, J., Jia, J., Zhang, B.: Fmm-yukawa: an adaptive fast multipole method for screened coulomb interactions. Comput. Phys. Commun. **180**(11), 2331–2338 (2009)